PROCEEDINGS OF SCIENCE

W and Z Physics

Christopher HAYS*
Oxford University
E-mail: hays@physics.ox.ac.uk

The electroweak theory elegantly combines the electromagnetic and weak forces, explaining a wide range of interactions using a gauge theory with just three parameters. The theory predicted the W and Z weak gauge bosons before they were directly observed in 1983, and its detailed predictions of W and Z boson properties have been tested to such precision that they now serve as probes for new particles through loop-level interactions. Currently, the limiting parameter in these probes is the W boson mass, whose uncertainty has been recently reduced by measurements of $\sqrt{s} = 1.96$ TeV $p\bar{p}$ collision data produced by the Fermilab Tevatron. Future measurements at the Tevatron and the Large Hadron Collider will result in nearly a factor of three reduction in the uncertainty on the W boson mass, significantly constraining the Higgs boson mass and the masses and couplings of supersymmetric particles. Other W and Z boson properties recently constrained by measurements at the Tevatron and HERA include their self-couplings and couplings to quarks.

European Physical Society Europhysics Conference on High Energy Physics
July 16-22, 2009
Krakow, Poland

*Speaker.

PoS(EPS-HEP 2009)016

1. The Electroweak Theory

All observed interactions can be described in terms of a gauge symmetry. The fundamental electroweak symmetry has the group structure $SU(2)_L \times U(1)_Y$ [1], but this symmetry is broken by the non-zero masses of the fermions and weak gauge bosons. In the Standard Model (SM), the vacuum expectation value (v) of the Higgs scalar field breaks the electroweak symmetry by fixing the relative direction between points in the $SU(2)_L$ and $U(1)_Y$ spaces. However, there is a residual rotational symmetry ($U(1)_{EM}$) that becomes the observed electromagnetic force.

Using this model, all known electroweak interactions are described with only three input parameters: the strengths of the $SU(2)_L$ (g) and $U(1)_Y$ (g') couplings, and the mass scale of the broken symmetry (v). The $SU(2)_L$ W and Z gauge bosons were discovered in 1983 [2], so the remaining unobserved particle of the model is the Higgs boson, whose discovery would confirm the details of symmetry breaking in the SM.

There is a wide range of electroweak observables that have been measured to high precision, determining the values of g, g', and v, and verifying the model's predictions. For example, the mixing between the two gauge groups is determined by the ratio of the couplings, which defines the Weinberg angle, $\theta_W = \tan^{-1}(g'/g)$, or $\sin^2\theta_W = g'^2/(g^2+g'^2)$. This angle and the fermion charges under $SU(2)_L$ and $U(1)_Y$ set the coupling between the Z boson and fermions. Since the weak gauge group $SU(2)_L$ couples only to left-handed fermions, Z boson production at e^+e^- and $p\bar{p}$ colliders results in an asymmetry between outgoing positively and negatively charged fermions, as a function of the angle with respect to the beam line. Measurements of these asymmetries at the Large Electron Positron collider (LEP) and the Stanford Linear Collider (SLC) have verified the predictions to high experimental precision [3].

The precision of the current measurements provides sensitivity to loop corrections from as-yet unobserved particles, such as the Higgs boson and supersymmetric particles [4]. The limiting uncertainty on this sensitivity comes from the measurement of the W boson mass (m_W). The tree-level relation, $m_W = gv/2$, predicts a W boson mass of 79.964 ± 0.005 GeV, whereas the current world average is 80.399 ± 0.023 GeV [5]. A significant correction to the tree-level prediction arises from the tb loop [6], and was used to predict the top quark mass before its discovery. An additional correction comes from Higgs boson loops, such that a factor of two increase in the Higgs boson mass reduces m_W by 41 MeV [7]. The current uncertainty on m_W from published measurements is 25 MeV [8], and a preliminary result from DØ [9] reduces the uncertainty to 23 MeV. A further reduction by a factor of three is expected from future measurements at the Tevatron and the Large Hadron Collider (LHC).

2. W Boson Mass Measurements and Constraints

The four experiments at LEP have published m_W measurements with precision ranging from $50-63$ MeV [10]. Final results are pending completion of studies into the effects of color reconnection. The current combined LEP measurement is $m_W = 80.376 \pm 0.033$ GeV.

The two Tevatron experiments have measured m_W in the three collider runs (0, I and II). The first Run II measurement has been published by the CDF Collaboration, with the result $m_W = 80.413 \pm 0.048$ GeV in 200 pb^{-1} of $\sqrt{s} = 1.96$ TeV $p\bar{p}$ collision data [8]. This is the single most

precise published measurement, recently surpassed by the preliminary DØ measurement of $m_W = 80.401 \pm 0.043$ GeV in 1 fb^{-1} of data [9]. Since the dominant uncertainties on these measurements are statistical, the precision is expected to significantly increase with the full Run II data set of $\mathcal{O}(10)$ fb^{-1}.

These measurements have been translated into constraints on the Higgs boson mass and supersymmetric particles. The results favor a low-mass Higgs boson, $m_H = 83^{+30}_{-23}$ GeV, when combined with other precision electroweak data [11].

2.1 Hadron-Collider Measurements

The m_W measurement at hadron colliders focuses on the electron and muon W-boson decay channels. Since the initial energy of the colliding partons is unknown, only momenta transverse to the beam line are used in the measurement. The neutrino momentum is inferred from the momentum imbalance in the event, and is combined with the charged-lepton momentum to calculate the transverse mass, $m_T = \sqrt{2p_T^l p_T^\nu (1-\cos\Delta\phi)}$, where $\Delta\phi$ is the angle between the leptons in the transverse plane.

The primary experimental issues are calibration of the charged-lepton momentum and the sources of the additional momenta in the event ('recoil'), from which the neutrino momentum is inferred. In the CDF measurement, muon momenta are measured with the tracker and calibrated with $J/\psi \to \mu\mu$, $\Upsilon \to \mu\mu$, and $Z \to \mu\mu$ resonances. Electron momenta are calibrated with the ratio of the measured energy in the calorimeter to the track momentum. The DØ measurement is based on the electron decay channel only, and uses $Z \to ee$ events for its electron and recoil calibrations. The CDF measurement relies on both $Z \to \mu\mu$ and $Z \to ee$ events for its recoil calibration. Since these calibrations are performed in-situ, their precision improves with statistics and will scale with increases in data.

Details of the production and decay of W bosons are external inputs to the m_W measurement, with uncertainties that do not directly scale with increasing statistics. However, the components based on non-perturbative QCD rely on parameters fit from data, and can thus become more precise with Tevatron measurements. Several measurements that reduce the uncertainty on m_W have recently been performed by the CDF and DØ experiments.

2.1.1 W Boson Production

The W-boson momentum is separately modelled in the longitudinal and the transverse directions. Along the beam axis, the momentum is determined by the fraction of (anti-)proton energy carried by the colliding partons. This fraction is predicted by the parton distribution functions (PDFs), which encapsulate the probability for a given parton to have a particular fraction of the (anti-)proton momentum. Parton distribution functions are defined at a low center-of-mass energy squared (Q^2) and evolved to higher Q^2 using the DGLAP equations [12]. Parameters in the functions are fit using a wide array of deep-inelastic scattering data. Perpendicular to the beam axis, the momentum is determined by QCD radiation that is calculable in the perturbative regime, and can otherwise be resummed to obtain a functional form with a few parameters fit from data.

W Boson Longitudinal Momentum

The *W* boson longitudinal momentum affects the m_W measurement through lepton acceptance. The CDF and DØ measurements accept electrons and muons in the central detector region, up to $|\eta| < 1.1$. In a decay with no *W*-boson momentum, the acceptance is purely determined by the decay angle. When there is longitudinal momentum, some leptons that would have been measured at the edges of the detector are no longer accepted, while others that would have been outside the detector are measured. Since the lepton p_T distribution is largely determined by the decay angle with respect to the beam line, the longitudinal momentum modifies the lepton p_T distribution and, in turn, the m_T distribution. In order to obtain the correct m_W in a fit, this effect must be correctly modelled. Uncertainties on the PDFs, which determine the boson longitudinal momentum, result in $\delta m_W = 13$ MeV for the CDF m_W measurement, and $\delta m_W = 9$ MeV for the DØ measurement obtained from a fit to the m_T distribution.

W bosons are predominantly produced via valence *u* and *d* quarks at the Tevatron (Fig. 1). The *u* quark has a higher fraction of the proton's momentum on average than the *d* quark, so W^+ bosons are produced with average longitudinal momentum in the direction of the proton momentum (and vice versa for W^- bosons, as shown in Fig. 2). This charge asymmetry as a function of longitudinal momentum has been measured at the Tevatron, constraining the ratio of u/d PDFs. Recent measurements of the *Z* boson rapidity also constrain the *u* and *d* PDFs.

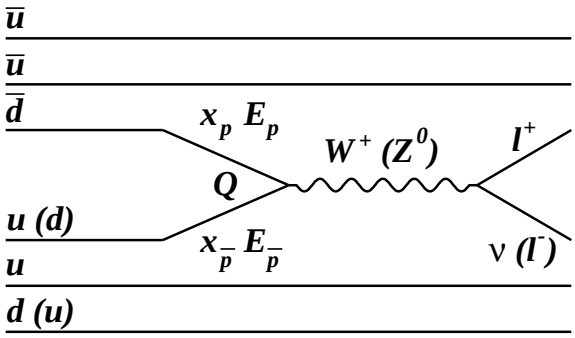

Figure 1: The dominant production mechanisms for *W* and *Z* bosons at the Tevatron.

W Boson Charge Asymmetry

DØ has recently measured the charge asymmetry of electrons from *W* boson decays, as a function of electron pseudorapidity [13]. The DØ measurement extends to $|\eta| < 3.2$, the widest coverage of such a measurement. In addition, DØ separates the electrons into two E_T bins, $25 < E_T < 35$ GeV and $E_T > 35$ GeV. The high-E_T bin has greater sensitivity to PDFs, since the decay direction tends to be transverse to the beam line, preserving the *W*-boson longitudinal momentum. At lower E_T the decay is closer to the beam line, and the left-handed coupling of the electron to the *W* boson results in a decay opposite to the direction of the *W*-boson longitudinal momentum. This effect counters the *W*-boson charge asymmetry, as shown in Fig. 2. The PDF uncertainty in the high-E_T region is thus considerably larger than in the low-E_T region, and will be significantly reduced by the DØ data (Fig. 3).

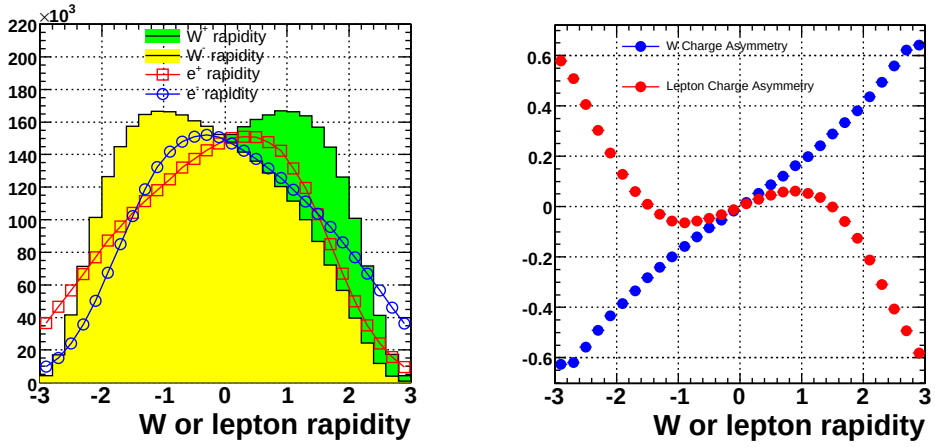

Figure 2: The W-boson and decay-electron rapidity distributions (left) and charge asymmetries (right) at the Tevatron.

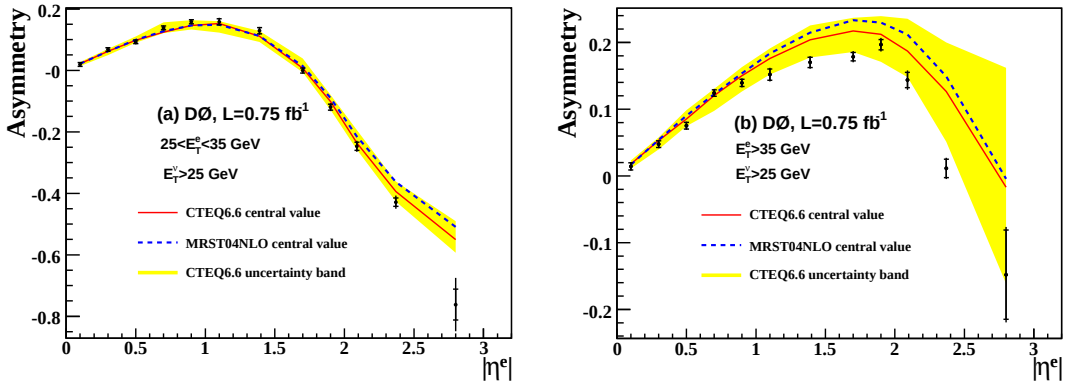

Figure 3: The measured charge asymmetry for electrons from W boson decays at DØ as a function of electron pseudorapidity.

To obtimize sensitivity to PDFs, CDF has applied a W-boson-mass constraint to the kinematics of each event and calculated two values of the longitudinal momentum of the neutrino. The values are assigned weights based on the measured and expected W-boson kinematic and decay distributions. Using these weighted solutions, the W boson charge asymmetry is directly determined up to boson rapidity $|y| < 3$ (Fig. 4) [14]. The measurement has higher precision than recent PDF fits from the CTEQ [15] and MRST [16] collaborations using next-to-leading order (NLO) and next-to-next-leading order (NNLO) QCD corrections, respectively.

Z Boson Rapidity

Measurements of Z bosons have the advantage of a fully reconstructable final state. The boson rapidity can be precisely measured and compared to predictions from PDFs. However, the $Z \to l^+l^-$ production cross section is about a factor of 10 lower than $W \to l\nu$ cross section. In addition,

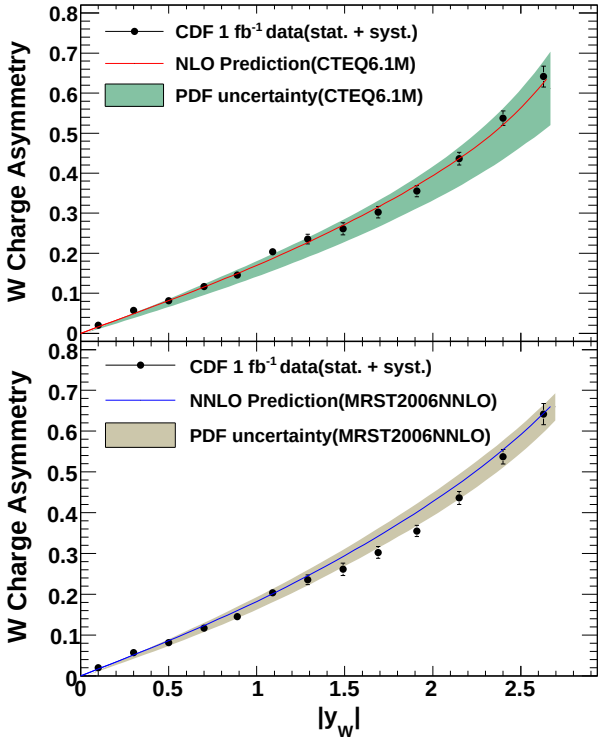

Figure 4: The measured charge asymmetry of W bosons at CDF, as a function of W boson rapidity.

the Z boson rapidity provides sensitivity to an average over all initial-state quarks, rather than the more specific sensitivity to u/d obtained from the W boson charge asymmetry.

CDF and DØ have measured the Z boson rapidity distribution using Run II data (Figs. 5 [17] and 6 [18]). The measurements currently have larger uncertainties than the PDFs, but could provide constraints with the full Run II data set.

W Boson Transverse Momentum

The W boson transverse momentum affects measurements of m_W that use the lepton p_T distributions. For these measurements, non-perturbative QCD radiation is the most relevant source of W boson p_T. CDF and DØ model p_T^W using the RESBOS [19] event generator, which is based on a next-to-leading log (NLL) calculation. The calculation has two parameters that are measured from data. The relevant parameter for measuring m_W is g_2, which determines the shape of the boson p_T as a function of center-of-mass energy. This parameter can be precisely measured using Z boson production at the Tevatron. The new DØ m_W measurement uses a value of g_2 obtained from a Z boson p_T measurement in DØ dielectron and dimuon data. The DØ p_T^Z measurement maximizes sensitivity to the non-perturbative parameters by defining two perpendicular axes, a_T and a_L, where a_T bisects the decay electrons. Figure 7 shows the shape of a_2 for two values of g_2. The measured a_T distributions and comparisons to prediction for $g_2 = 0.63$ are shown in Fig. 8.

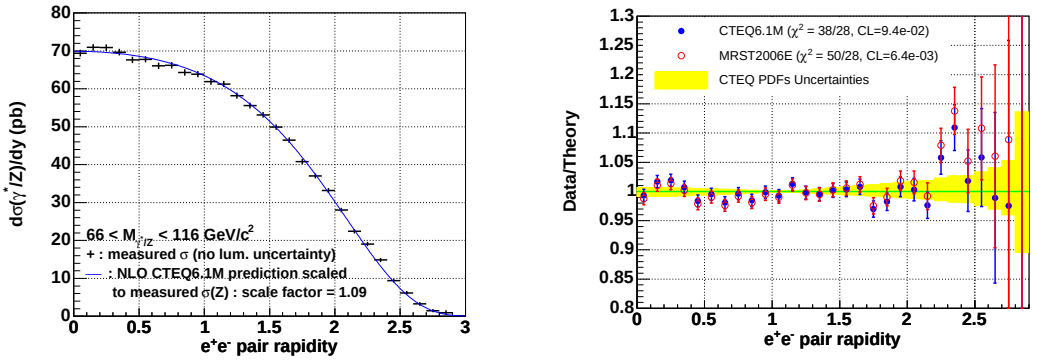

Figure 5: The Z boson rapidity distribution measured by CDF (left) and the ratio with respect to prediction (right).

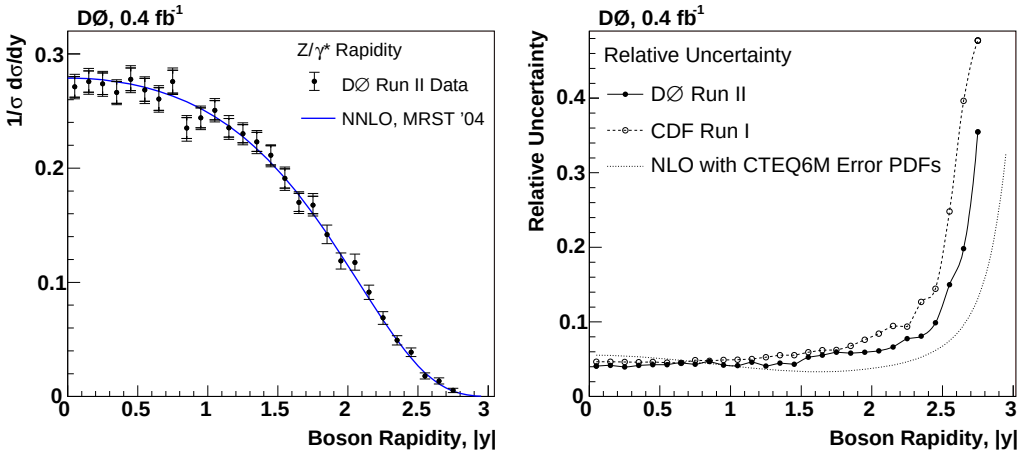

Figure 6: The Z boson rapidity distribution measured by DØ (left) and the relative uncertainties compared to the CDF Run I prediction and the PDF uncertainties determined by CTEQ (right).

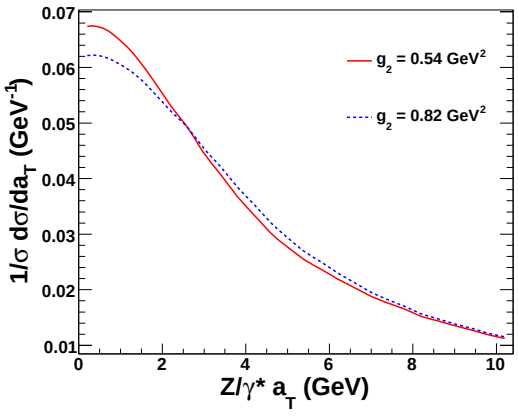

Figure 7: The Z boson a_T distribution for two values of the g_2 parameter.

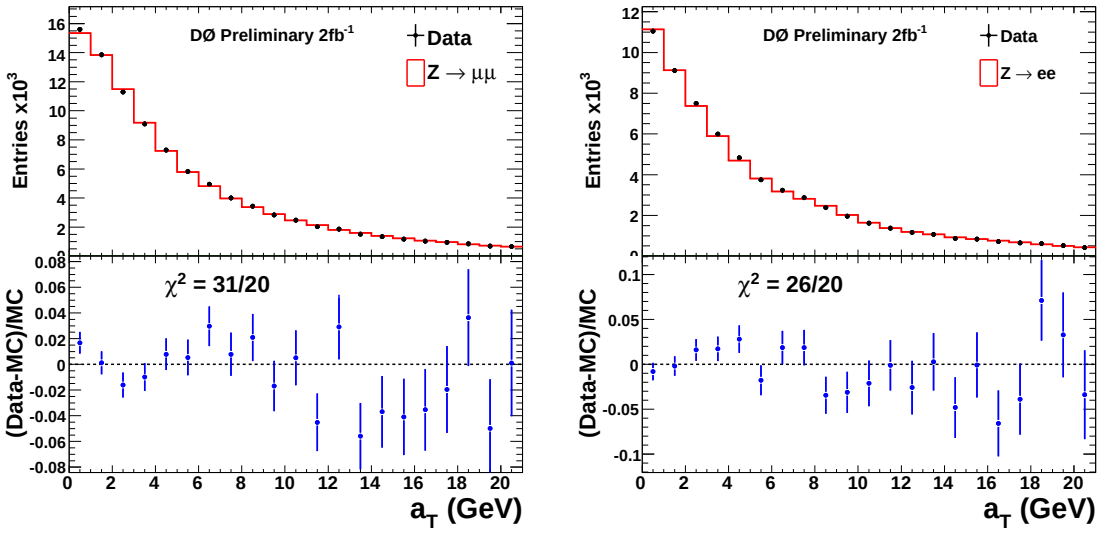

Figure 8: The distributions of Z-boson a_T measured by DØ compared to the prediction for $g_2 = 0.63$.

2.1.2 *W* Boson Decay

Initial-state QCD radiation affects the W-boson polarization, and thus the decay-angle distribution. This distribution is modelled with RESBOS using the NLO prediction. Final-state photon radiation from the charged lepton reduces the measured m_T and would cause an $\mathcal{O}(150$ MeV) bias if it were not accounted for. DØ models this radiation with PHOTOS [20], which calculates the leading-logarithmic contributions, and compares to a next-to-leading order calculation implemented in WGRAD [21]. A combined NLO-LL calculation has been implemented in HORACE [22], promising a reduced uncertainty in future measurements. Current uncertainties from QED radiation are $\delta m_W = 12$ MeV for the CDF m_W measurement and $\delta m_W = 7$ MeV for the DØ m_W measurement.

2.1.3 DØ *W* Boson Mass Measurement

The DØ m_W measurement calibrates the detector response to electrons using a sample of 18,725 $Z \to ee$ events. Using the precisely known Z-boson mass, DØ obtains a scale and an offset of the measured energy with respect to the true energy. Figure 9 shows the Z boson mass after the calibration.

A model of the detector response to the remaining particles in a W-boson event, from which the neutrino transverse momentum is inferred, is developed using GEANT [23] and events collected at a fixed rate from a zero-bias trigger. The parameters of the model are tuned with $Z \to ee$ events. As with the electron energy calibration, the precision of the neutrino calibration is determined by Z boson statistics and will improve with additional data.

The m_W fits to the W-boson m_T (Fig. 10), p_T^e, and p_T^ν distributions result in a combined measurement of $m_W = 80.401 \pm 0.021_{stat} \pm 0.038_{sys}$. Table 1 show the uncertainties associated with each fit. With a total uncertainty of 43 MeV, this is currently the single most precise m_W measurement.

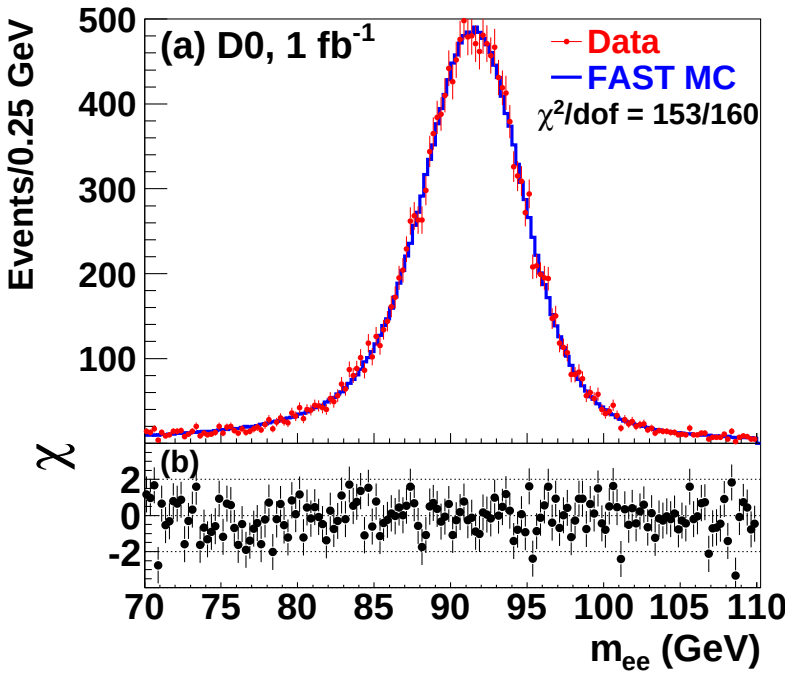

Figure 9: The measured dielectron mass spectrum and comparison to prediction after electron energy calibration.

	δm_W (MeV)		
Source	m_T	p_T^e	p_T^ν
Electron energy calibration	34	34	34
Electron resolution model	2	2	3
Electron shower modeling	4	6	7
Electron energy loss model	4	4	4
Hadronic recoil model	6	12	20
Electron efficiencies	5	6	5
Backgrounds	2	5	4
Experimental Subtotal	35	37	41
PDF	10	11	11
QED	7	7	9
Boson p_T	2	5	2
Production Subtotal	12	14	14
Total	37	40	43

Table 1: Systematic uncertainties on the DØ m_W measurement.

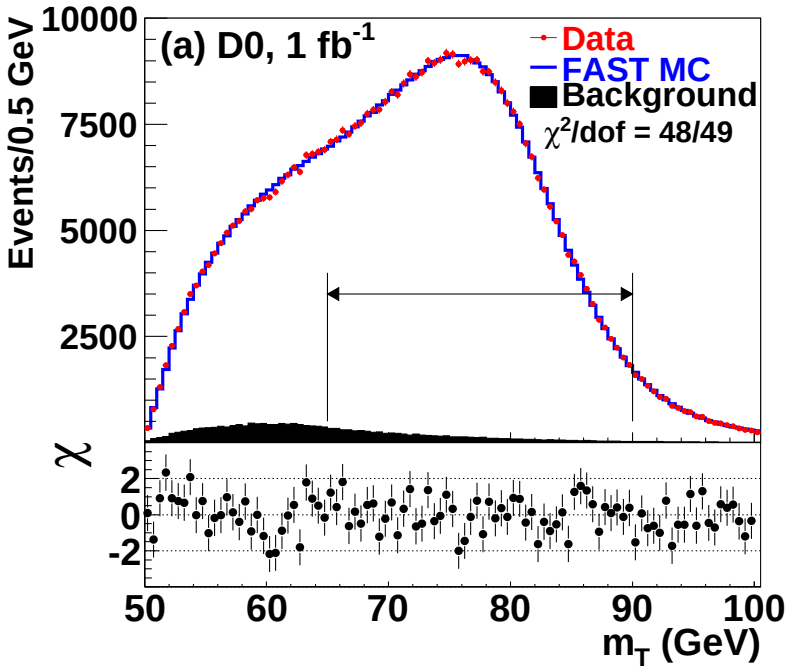

Figure 10: The m_T spectrum measured by DØ compared to prediction after fitting for m_W.

2.1.4 Future Measurements

Given recent measurements and theoretical developments that improve the W-boson production model at the Tevatron, future m_W measurements by CDF and DØ are expected to have significantly reduced uncertainties. Measurements with precision better than 25 MeV are expected with 2.3 (5.0) fb^{-1} of CDF (DØ) data. At the LHC, the ATLAS experiment expects to measure m_W to 7 MeV precision with 45 (4.5) million W (Z) boson events collected in 10 fb^{-1} of data [24].

2.2 Constraints

The DØ m_W measurement has been combined with previous Tevatron measurements to produce a new Tevatron average of $m_W = 80.420 \pm 0.031$ GeV [5]. The 31-MeV precision exceeds that of LEP, whose combined average of four experiments is $m_W = 80.376 \pm 0.033$ GeV.

The Gfitter collaboration has incorporated the new DØ measurement into its global electroweak fits [11]. The inferred Higgs boson mass is $m_H = 83^{+30}_{-23}$ (Fig. 11), more than 1σ below the direct limit from LEP [25]. The m_W measurement alone prefers a lower mass Higgs boson, 42^{+56}_{-22}. If the mass value does not change with more precise measurements, the consistency with the SM would decrease, suggesting the presence of new particles coupling to the W boson (Fig. 12 [4]). There is one 2.5σ outlier in the m_H fit: the measurement of the forward-backward asymmetry of b-quark production in polarized beams at SLC [3]. The Gfitter group finds a 1.4% probability to find an outlier at least as deviant as this one, assuming no new physics beyond the SM.

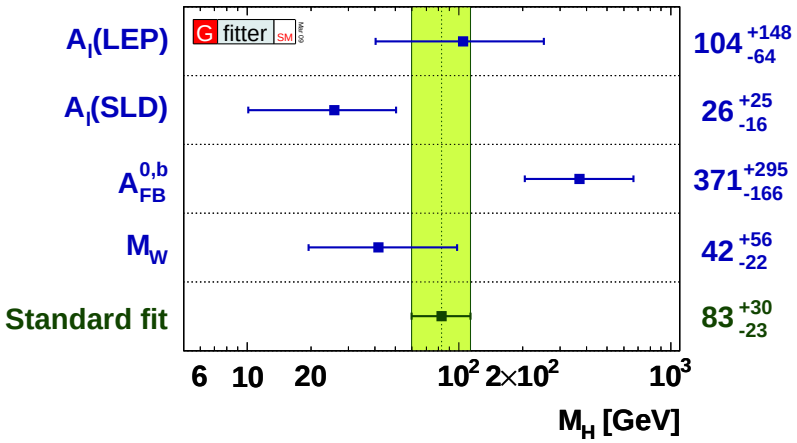

Figure 11: The Gfitter determination of the Higgs boson mass from individual measurements and from the combined electroweak measurements.

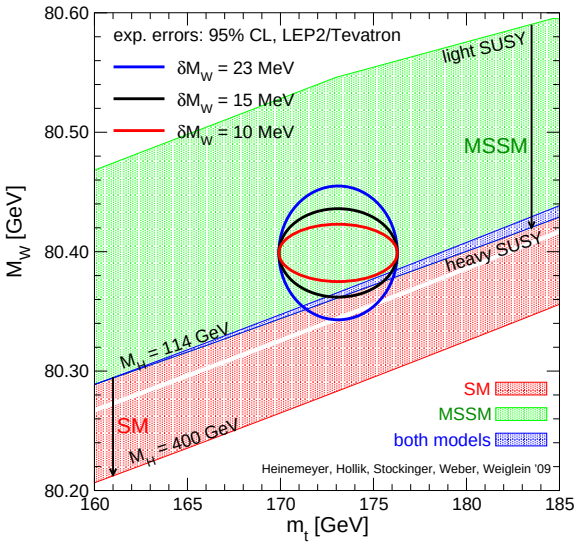

Figure 12: The best-fit W-boson and top-quark masses, with 95% uncertainty ellipses for various m_W uncertainties. The hashed regions show the SM range of m_W and m_t for various values of the Higgs boson mass, and the corresponding range in the minimal supersymmetric model (MSSM).

3. Measurements of Gauge-Boson Couplings

The electroweak gauge-boson self-couplings and couplings to fermions have been measured to high precision at LEP and SLC. These experiments have directly measured these couplings up to the kinematic limit of 209 GeV center-of-mass energy. Studies of gauge-boson couplings at HERA and the Tevatron directly probe these couplings to higher center-of-mass energies, and are thus sensitive to deviations from the SM at higher mass scales.

3.1 Forward-Backward Asymmetry at the Tevatron

The scattering amplitude for the $f\bar{f} \to e^- e^+$ process is [26]

$$A_{ij} = A(f_i \bar{f} \to e_j^- e^+) = -Qe^2 + \frac{\hat{s}}{\hat{s} - m_Z^2 + im_Z\Gamma_Z} C_i(f) C_j(e), \tag{3.1}$$

where i and j are the fermion helicities (L,R), Q is the electromagnetic charge of fermion f, $C_{i,j}(f)$ are the fermion couplings to the Z boson, m_Z (Γ_Z) is the Z boson mass (width), and $\hat{s}$ is the squared center-of-mass energy of the collision. Using this amplitude, the differential angular cross section is

$$\frac{d\sigma}{d\cos\theta^*} = \frac{1}{128\pi\hat{s}}[(|A_{LL}|^2 + |A_{RR}|^2)(1+\cos\theta^*)^2 + (|A_{LR}|^2 + |A_{RL}|^2)(1-\cos\theta^*)^2], \tag{3.2}$$

where θ^* is the angle of the electron with respect to the incoming proton direction in the boson rest mass frame. By measuring the difference in cross section between positive and negative $\cos\theta^*$ (forward and backward electron directions) as a function of invariant mass, the fermion couplings to the Z boson can be measured. Writing the vector (v_f) and axial (a_f) couplings as,

$$v_f = I_L^3 - 2e\sin^2\theta_W \tag{3.3}$$

$$a_f = I_L^3, \tag{3.4}$$

where I_L^3 is the fermion weak charge, measurements of the couplings determine $\sin^2\theta_W$.

DØ has performed a measurement of the electron forward-backward asymmetry (A_{FB}) with 1.1 fb^{-1} of dielectron data (Fig. 13), and extracted $\sin^2\theta_W$ from the measurement [27]. The result of $\sin^2\theta_W = 0.2326 \pm 0.0018_{stat} \pm 0.0006_{sys}$ can be compared to the SM value determined from previous measurements, $\sin^2\theta_W = 0.23149 \pm 0.00013$. While the DØ measurement is ≈ 10 times less precise than the SM value, a combined dielectron and dimuon measurement with the full Run II data set for CDF and DØ could give precision within a factor of ≈ 3 of the SM value.

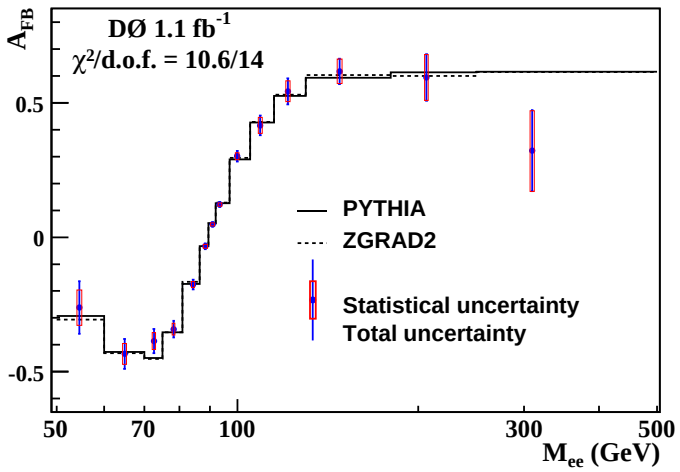

Figure 13: The forward-backward asymmetry A_{FB} of electrons in 1.1 fb^{-1} of DØ $e^- e^+$ data, as a function of dielectron mass.

3.2 Global Fits at HERA

Data from electron-proton collisions at HERA are used to determine the quark axial and vector couplings to the neutral current through measurements of $eq \to eq$ inelastic scattering [28]. The data are fit globally for PDF and electroweak parameters and resolve the (v_q, a_q) sign ambiguity from LEP measurements. Results from fits to the HERA data are shown in Fig. 14, along with CDF and LEP measurements. The HERA results are the most precise, and the experiments have a factor of two more data available to increase the precision. The CDF result uses 72 pb^{-1} of data [29]; analysis of the significantly larger available data set would make the Tevatron experiments competitive in this measurement.

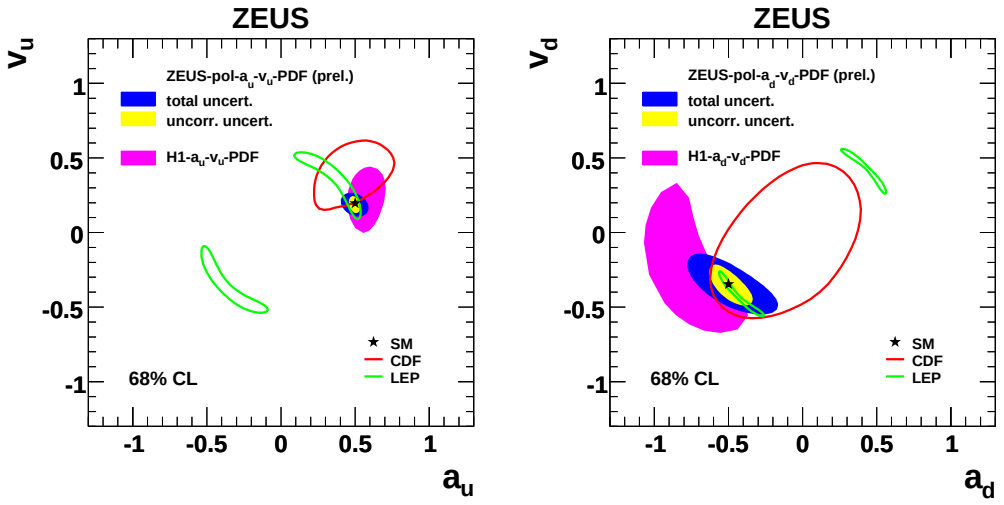

Figure 14: The axial and vector couplings of up (left) and down (right) quarks to Z bosons, as predicted by the SM and measured by ZEUS, H1, CDF, and LEP.

3.3 Diboson Production at Hadron Colliders

Boson pair production at the Tevatron includes a small $\mathcal{O}(10\%)$ contribution from vertices with three gauge bosons (triple-gauge couplings). Studies of these processes provide sensitivity to non-SM couplings at high center-of-mass energies, including the only tests of individual $WW\gamma$ and WWZ vertices. Single-boson production at HERA is sensitive to triple-gauge couplings through the vector-boson fusion process, where the incoming quark and electron radiate gauge bosons that fuse into a single gauge boson.

3.3.1 Final States with Photons

CDF and DØ have measured the $W\gamma$ and $Z\gamma$ production cross sections and set limits on non-SM ('anomalous') couplings. A new DØ study of $Z \to \nu\nu + \gamma$ production in 3.6 fb^{-1} of data [30] is sensitive to the presence of a $ZZ\gamma$ vertex, which does not exist in the SM. The observed photon E_T distribution is consistent with the SM prediction (Fig. 15).

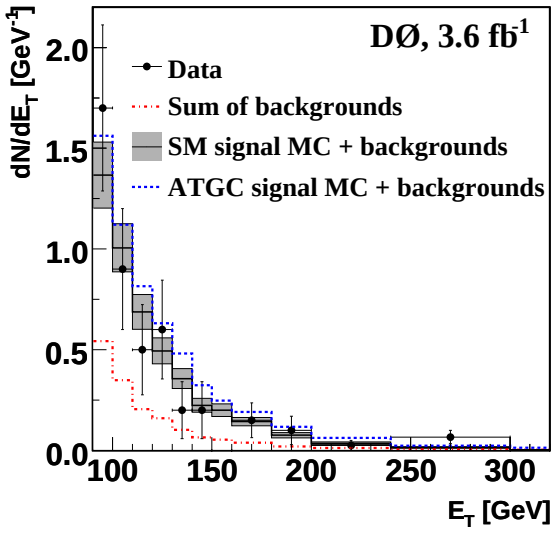

Figure 15: The observed photon E_T spectrum in $Z \to \nu\nu + \gamma$ events, compared to SM expectation and a model with anomalous triple-gauge couplings (ATGC).

3.3.2 Fully Leptonic Final States

CDF has updated its measurement of the $WW \to l\nu l\nu$ production cross section with 3.6 fb^{-1} of data and set limits on anomalous $WW\gamma$ and WWZ couplings. The measurement of $\sigma(p\bar{p} \to WW) = 12.1 \pm 0.9(\text{stat}) \,^{+1.6}_{-1.4}(\text{sys})$ is consistent with the SM prediction of 11.7 ± 0.7 pb. Figure 16 shows the p_T distribution of the highest p_T charged lepton in $WW \to l\nu l\nu$ candidate events.

CDF and DØ have made the first observations of ZZ production at a hadron collider. Combining $ZZ \to llll$ and $ZZ \to ll\nu\nu$ signatures, CDF obtains a 4.4σ excess over background [31], while DØ observes ZZ production with 5.7σ significance [32].

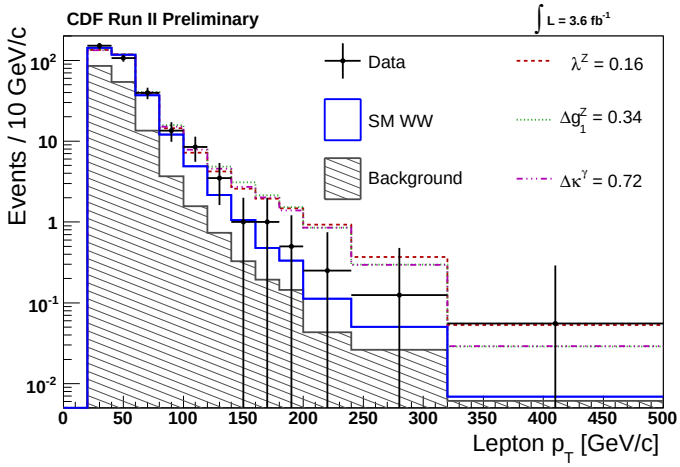

Figure 16: The observed charged lepton p_T spectrum in $W \to l\nu l\nu$ events, compared to SM expectation and two models with anomalous triple-gauge couplings (ATGC) that the data exclude at 95% confidence level.

3.3.3 Final States with Jets

The Tevatron experiments are making their first observations of heavy-boson decays to quark pairs. DØ has observed 4.4σ evidence for $WW/WZ \to l\nu qq$ production (Fig. 17) [33], and set limits on anomalous couplings. CDF has made a 5.3σ observation of $WZ/ZZ \to qq\nu\nu$ production (Fig. 18) [34].

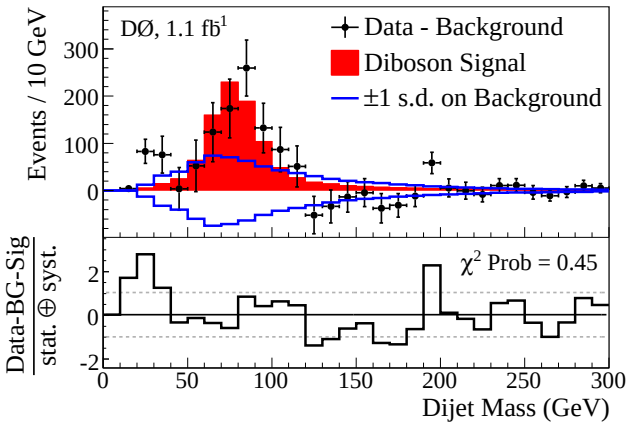

Figure 17: The background-subtracted dijet mass distribution in 1.1 fb^{-1} of DØ data. The peak centered on ≈ 80 GeV represents $WW/WZ \to l\nu qq$ signal, with a 4.4σ-significant excess above the background.

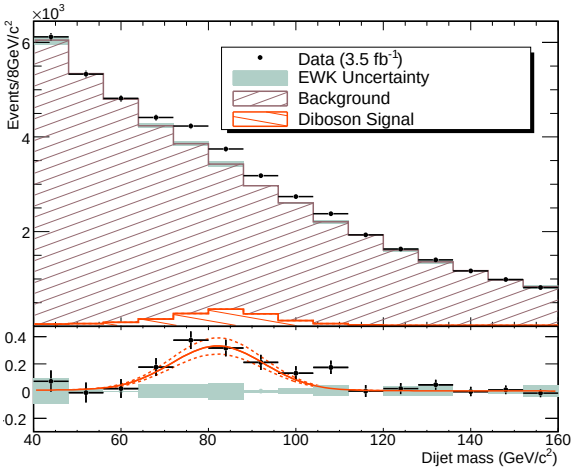

Figure 18: The observed CDF dijet mass distribution in events with significant momentum imbalance. Events from the processes $WZ/ZZ \to qq\nu\nu$ are clearly distinguished by their invariant masses close to m_W and m_Z.

3.4 *W* Boson Production at HERA

H1 has measured the cross section of W boson production in $\sqrt{s} = 317$ GeV ep collisions (Fig. 19) [35]. The cross section includes production via vector-boson fusion (Fig. 20), where the electron radiates a photon and the quark radiates a W boson, and the two bosons fuse into a

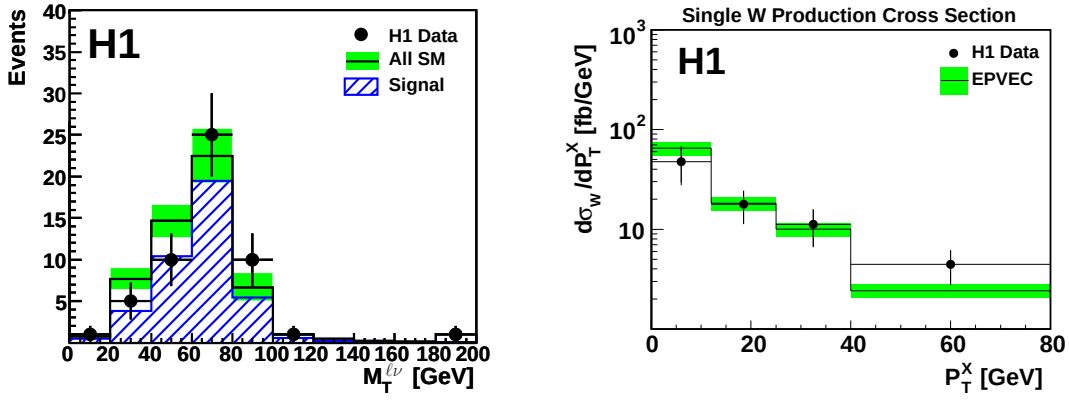

Figure 19: The observed m_T distribution (left) and the measured W boson production cross section as a function of the hadronic recoil momentum P_T^X.

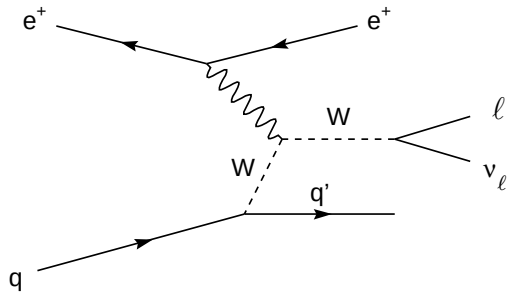

Figure 20: The Feynman diagram for the production of W bosons via vector-boson fusion in ep collisions.

W boson. The measurement has been used to set limits on anomalous $WW\gamma$ couplings, and to demonstrate the presence of this coupling in W boson production at 95% confidence level.

4. Conclusions

Ongoing measurements at the Tevatron and HERA are making significant progress in probing the electroweak theory at the loop level, and in testing the non-Abelian electroweak gauge structure. Measurements of the W boson mass at CDF and DØ are constraining the mass of the Higgs boson and the properties of hypothetical particles. Future measurements from these experiments and at the LHC promise a factor ≈ 3 improvement in precision on m_W. Ongoing electroweak measurements at the Teavtron are reducing the systematic uncertainties on input parameters for the m_W measurement. In addition, triple-gauge couplings are being studied in new production and decay modes, in particular hadronic decay modes at the Tevatron and the vector-boson fusion production mode at HERA. With significant quantities of data still to be analyzed, the Tevatron and HERA experiments will continue to test the SM to unprecendented levels.

References

[1] S. Glashow, Nucl. Phys. **22**, 579 (1967); S. Weinberg, Phys. Lett. **12**, 132 (1967); A. Salam, *Elementary Particle Physics*, N. Svartholm ed., 367 (1968).

[2] G. Arnison *et al.* (UA1 Collaboration), Phys. Lett. B **122**, 103 (1983); M. Banner *et al.* (UA2 Collaboration), Phys. Lett. B **122**, 476 (1983); G. Arnison *et al.* (UA1 Collaboration), Phys. Lett. B **126**, 398 (1983); P. Bagnaia *et al.* (UA2 Collaboration), Phys. Lett. B **129**, 130 (1983).

[3] S. Schael *et al.* (ALEPH, DELPHI, L3, OPAL, and SLD Collaborations), Phys. Rep. **427**, 257 (2006).

[4] S. Heinemeyer *et al.*, J. High Energy Phys. **08**, 052 (2006).

[5] Tevatron Electroweak Working Group, *arXiv:0908.1374* (2009).

[6] D. C. Kennedy and B. W. Lynn, Nucl. Phys. **B322**, 1 (1989); M. B. Einhorn, D. R. T. Jones, and M. Veltman, Nucl. Phys. **B191**, 146 (1981).

[7] M. Awramik, M. Czakon, A. Freitas, and G. Weiglin, Phys. Rev. D **69**, 053006 (2004).

[8] T. Aaltonen *et al.* (CDF Collaboration), Phys. Rev. D **77**, 112001 (2008).

[9] V. M. Abazov *et al.* (DØ Collaboration), *arXiv:0908.0766v1* (2009).

[10] S. Schael *et al.* (ALEPH Collaboration), Eur. Phys. J. C **47**, 309 (2006); G. Abbiendi *et al.* (OPAL Collaboration), Eur. Phys. J. C **45**, 307 (2006); P. Achard *et al.* (L3 Collaboration), Eur. Phys. J. C **45**, 569 (2006); J. Abdallah *et al.* (DELPHI Collaboration), submitted to Z. Phys. C.

[11] H. Flächer *et al.* (Gfitter Collaboration), Eur. Phys. J. C **60**, 543 (2009).

[12] V. N. Gribov and L. N. Lipatov, Sov. J. Nucl. Phys. **15**, 438 (1972); G. Altarelli and G. Parisi, Nucl. Phys. **B126**, 298 (1977); Y. L. Dokshitzer, Sov. Phys. JETP **46**, 641 (1977).

[13] V. M. Abazov *et al.* (DØ Collaboration), Phys. Rev. Lett. **101**, 211801 (2008).

[14] T. Aaltonen *et al.* (CDF Collaboration), Phys. Rev. Lett. **102**, 181801 (2009).

[15] J. Pumplin *et al.*, J. High Energy Phys. 0207, 012 (2002).

[16] A. D. Martin, R. G. Roberts, W. J. Stirling, and R. S. Thorne, Eur. Phys. J. C **28**, 455 (2003).

[17] T. Aaltonen *et al.* (CDF Collaboration), *arXiv:0908.3914* (2009).

[18] V. M. Abazov *et al.* (DØ Collaboration), Phys. Rev. D **76**, 012003 (2007).

[19] F. Landry, R. Brock, P.M. Nadolsky, and C.-P. Yuan, Phys.Rev. D **67**, 073016 (2003); C. Balazs and C.-P. Yuan, Phys.Rev. D **56**, 5558 (1997); G.A. Ladinsky and C.-P. Yuan, Phys.Rev. D **50**, R4239 (1994).

[20] E. Barbiero and Z. Was, Comput. Phys. Commun. **79**, 291 (1994).

[21] U. Baur, S. Keller, and D. Wackeroth, Phys. Rev. D **59**, 013002 (1998).

[22] C. M. Carloni Calame *et al.*, Phys. Rev. D **69**, 037301 (2004).

[23] R. Brun and F. Carminati, CERN Program Library Long Writeup W5013 (1993).

[24] G. Aad *et al.* (ATLAS Collaboration), *arXiv:0901.0512* (2009).

[25] R. Barate *et al.* (ALEPH, DELPHI, L3, and OPAL Collaborations), Phys. Lett. B *565*, 61 (2003).

[26] J. L. Rosner, Phys. Rev. D **54**, 1078 (1996).

[27] V. M. Abazov *et al.* (DØ Collaboration), Phys. Rev. Lett. **101**, 191801 (2008).

[28] A. Aktas *et al.* (H1 Collaboration), Phys. Lett. B **632**, 35 (2006).

[29] D. Acosta *et al.* (CDF Collaboration), Phys. Rev. D **71**, 052002 (2005).

[30] V. M. Abazov *et al.* (DØ Collaboration), Phys. Rev. Lett. **102**, 201802 (2009).

[31] T. Aaltonen *et al.* (CDF Collaboration), Phys. Rev. Lett. **100**, 201801 (2008).

[32] V. M. Abazov *et al.* (DØ Collaboration), Phys. Rev. Lett. **101**, 171803 (2008).

[33] V. M. Abazov *et al.* (DØ Collaboration), Phys. Rev. Lett. **102**, 161801 (2009).

[34] T. Aaltonen *et al.* (CDF Collaboration), Phys. Rev. Lett. **103**, 091803 (2009).

[35] F. D. Aaron *et al.* (H1 Collaboration), *arXiv:0901.0488* (2009).